AGU PUBLICATIONS

Water Resources Research

RESEARCH ARTICLE
10.1002/2014WR015388

Key Points:
- Specific interfacial area depends on dynamic conditions
- Interfacial velocity and production term show similar trends
- Further investigation of the dynamic conditions and of all interfaces is needed

Correspondence to:
N. K. Karadimitriou,
N.K.Karadimitriou@uu.nl

Citation:
Karadimitriou, N. K., S. M. Hassanizadeh, V. Joekar-Niasar, and P. J. Kleingeld (2014), Micromodel study of two-phase flow under transient conditions: Quantifying effects of specific interfacial area, *Water Resour. Res.*, *50*, 8125–8140, doi:10.1002/2014WR015388.

Received 30 JAN 2014
Accepted 20 SEP 2014
Accepted article online 24 SEP 2014
Published online 21 OCT 2014

Micromodel study of two-phase flow under transient conditions: Quantifying effects of specific interfacial area

N. K. Karadimitriou[1], S. M. Hassanizadeh[1], V. Joekar-Niasar[2], and P. J. Kleingeld[1]

[1]Earth Sciences Department, Utrecht University, Utrecht, Netherlands, [2]School of Chemical Engineering and Analytical Science, The University of Manchester, Manchester, United Kingdom

Abstract Recent computational studies of two-phase flow suggest that the role of fluid-fluid interfaces should be explicitly included in the capillarity equation as well as equations of motion of phases. The aim of this study has been to perform experiments where transient movement of interfaces can be monitored and to determine interfacial variables and quantities under transient conditions. We have performed two-phase flow experiments in a transparent micromodel. Specific interfacial area is defined, and calculated from experimental data, as the ratio of the total area of interfaces between two phases per unit volume of the porous medium. Recent studies have shown that all drainage and imbibition data points for capillary pressure, saturation, and specific interfacial area fall on a unique surface. But, up to now, almost all micromodel studies of two-phase flow have dealt with quasi-static or steady state flow conditions. Thus, only equilibrium properties have been studied. We present the first study of two-phase flow in an elongated PDMS micromodel under transient conditions with high temporal and spatial resolutions. We have established that different relationships between capillary pressure, saturation, and specific interfacial area are obtained under steady state and transient conditions. The difference between the surfaces depends on the capillary number. Furthermore, we use our experimental results to obtain average (macroscale) velocity of fluid-fluid interfaces and the rate of change of specific interfacial area as a function of time and space. Both terms depend on saturation nonlinearly but show a linear dependence on the rate of change of saturation. We also determine macroscale material coefficients that appear in the equation of motion of fluid-fluid interfaces. This is the first time that these parameters are determined experimentally.

1. Introduction

1.1. Specific Interfacial Area and Two-Phase Flow

A cornerstone of theories of two-phase flow in porous media is the capillary pressure-saturation, P^c-S, relationship. It actually relates the difference in macroscale pressures of two immiscible fluids to the saturation of one of the fluids. Almost always, it is measured under static conditions, and then it is used to model transient conditions. It is well known that this relationship is hysteretic, and does not explicitly include any information on the dynamics of the interfaces formed between the two phases. One may get many capillary pressure-saturation curves, for the same porous medium and the same set of phases, but for different initial conditions and/or different displacement processes. Following an approach based on volume averaging and rational thermodynamics, *Hassanizadeh and Gray* [1990, 1993b] developed a macroscale theory of two-phase flow. Using the volume averaging approach, they derived macroscale balance laws for masses, momenta, energies, and entropies of fluid-fluid and fluid-solid interfaces [*Gray and Hassanizadeh*, 1989]. Their derivation made it clear that in multiphase flow, one must take account of the thermodynamics of interfaces among phases in order to be able to describe physicochemical processes in porous media. In particular, they derived the following equation of mass balance for the interfacial mass between phases α and β.

$$\frac{\partial a^{\alpha\beta}\Gamma^{\alpha\beta}}{\partial t} + \overrightarrow{\nabla}\left(a^{\alpha\beta}\Gamma^{\alpha\beta}\overrightarrow{w}^{\alpha\beta}\right) = \mathrm{E}^{\alpha}_{\alpha\beta} + \mathrm{E}^{\beta}_{\alpha\beta} + \mathrm{E}_{\alpha\beta\gamma} \tag{1}$$

where $a^{\alpha\beta}$ [L^{-1}] is called specific interfacial area between α and β phases. It is defined as the total area of $\alpha\beta$ interfaces within an REV divided by the volume of the REV. An REV (Representative Elementary Volume) of a (macroscopically) homogeneous porous medium is the averaging volume for which the system properties are insensitive to the changes in the averaging domain size. Further, $\Gamma^{\alpha\beta}$ [ML^{-2}] is the macroscale interfacial

mass density, defined as the total mass of all interfaces within an REV divided by the sum of areas of those interfaces. The term $a^{\alpha\beta}\Gamma^{\alpha\beta}\overrightarrow{w}^{\alpha\beta}$ represents the total mass flux of interfaces within an REV, where $\overrightarrow{w}^{\alpha\beta}$ [LT^{-1}] is the average velocity of those interfaces. The latter term ($\overrightarrow{w}^{\alpha\beta}$) also represents the momentum associated with interfaces per unit mass. Finally, the terms on the right-hand side of equation (1) account for the exchange of mass between $\alpha\beta$ interfaces and the α-phase, β-phase, and $\alpha\beta\gamma$-contact lines. It must be stressed that all terms in equation (1) are macroscopic (i.e., REV-averaged) quantities. Similar balance laws were derived for momentum, energy, and entropy of interfaces by *Marle* [1982] and *Gray and Miller* [2006].

The explicit introduction of interfacial properties into the theories of multiphase flow was a major departure from traditional theories of two-phase flow in porous media. Specific interfacial area was considered to be a state variable needed for the description of fluid flow dynamics. Balance laws were complemented by constitutive equations and, by employing the rational thermodynamics approach; *Hassanizadeh and Gray* [1990] derived Darcy-type equations for macroscale velocities of phases and interfaces. In particular, the following linear approximation was developed for the average velocity of fluid-fluid interfaces [see, e.g., *Hassanizadeh and Gray*, 1993b]:

$$\overleftrightarrow{R}^{wn}\overrightarrow{w}^{wn}=\overrightarrow{\nabla}(a^{wn}\cdot\sigma^{wn})+\Psi^{wn}\overrightarrow{\nabla}S^{w} \tag{2}$$

where superscripts w and n denote wetting and nonwetting phases, respectively, $\overleftrightarrow{R}^{wn}$ [$ML^{-3}T^{-1}$] is a resistance tensor, σ^{wn} [MT^{-2}] is the interfacial tension of wn-interface, S^{w} is the wetting phase saturation, Ψ^{wn} [$ML^{-1}T^{-2}$] is a material coefficient, which may be a function of S^{w} and a^{wn}.

Equations (1) and (2) can be simplified if we assume that the interfacial mass density $\Gamma^{\alpha\beta}$ and interfacial tension σ^{wn} are constant. This is a reasonable assumption for isothermal situations and in the absence of surfactants. For the sake of the current study, we consider one-dimensional flow on the macroscale. As a result, equations (1) and (2) can be recast in the following forms [see, e.g., *Niessner and Hassanizadeh*, 2009]:

$$\frac{\partial a^{wn}}{\partial t}+\frac{\partial}{\partial x}(a^{wn}w^{wn})=E^{wn} \tag{3}$$

$$w^{wn}=-k^{wn}\left(\frac{\partial a^{wn}}{\partial x}+\psi^{wn}\frac{\partial S^{w}}{\partial x}\right) \tag{4}$$

where E^{wn} [$L^{-1}T^{-1}$] is the rate of production of fluid-fluid interfaces, k^{wn} [$L^{3}T^{-1}$] is the interfacial conductivity coefficient, and ψ^{wn} [L^{-1}] is a material coefficient. All three parameters may still depend on S^{w} and a^{wn}.

In addition to governing equations for specific interfacial area, the rational thermodynamics approach also led to new hypothesis for the capillary pressure. Results of the constitutive theory suggested that the capillary pressure is not only a function of saturation, but should also depend on specific interfacial area [*Hassanizadeh and Gray*, 1993a].They postulated that the hysteretic behavior of P^{c}-S^{w} relationship, where P^{c} stands for capillary pressure, can be modeled by introducing fluid-fluid specific interfacial area as an additional state variable. Based on this hypothesis, capillary pressure-saturation-specific interfacial area data points from drainage and imbibition processes would fall on a unique surface. Such a surface can be described by the following formula:

$$a^{wn}=a^{wn}(P^{c},S^{w}) \tag{5}$$

Henceforth, we refer to P^{c}-S^{w}-a^{wn} surface as the "interfacial area surface." Also, unless otherwise stated with the term "saturation," we refer to the wetting phase saturation.

A growing number of numerical and experimental works have shown that under quasi-static conditions, drainage and imbibition interfacial area surfaces (formed by data points from drainage and imbibition experiments, respectively) coincide with each other, within the margin of experimental error. The earliest studies were done by *Reeves and Celia* [1996], and *Held and Celia* [2001], who performed quasi-static pore-network modeling and showed the uniqueness of interfacial area surface. A similar result was obtained by *Porter et al.* [2009] using a Lattice-Boltzmann model. The first experimental evidence for the uniqueness of interfacial area surface was provided by *Cheng et al.* [2004] and later by *Chen et al.* [2007] and *Pyrak-Nolte et al.* [2008]. They performed two-phase flow experiments in a micromodel. A combination of pore-network modeling and micromodel experimental studies was performed by *Joekar-Niasar et al.* [2009a, 2009b] and

more recently by *Karadimitriou et al*. [2013]. All these studies have one thing in common; they considered quasi-static conditions only. Under quasi-static conditions, the fluid-fluid interfaces do not move in the porous medium.

The question one may ask is whether an interfacial area surface can be obtained under different transient flow conditions, and if yes, whether it would coincide with quasi-static interfacial area surface. These questions were recently addressed by *Bottero* [2009] and *Joekar-Niasar and Hassanizadeh* [2012]. *Bottero* [2009] performed experiments in a small micromodel (network dimensions were 0.6 mm by 0.6 mm). The two fluid phases were decane and nitrogen gas. She determined the average capillary pressure for the whole network based on the average of curvatures of all interfaces within the network. The curvatures were obtained from image analysis. Images were also used to determine network-scale saturation and interfacial area. These quantities were obtained as a function of time in the case of transient experiments. She compared the interfacial surfaces obtained under quasi-static and transient conditions and concluded that the differences were within measurement errors [*Bottero*, 2009, chap. 8]. One shortcoming of her study was that the micromodel network size was too small; thus, boundaries may have affected the results. *Joekar-Niasar and Hassanizadeh* [2012] investigated the above mentioned questions in a numerical study, using a dynamic pore-network model. They determined the average capillary pressure, saturation, and specific interfacial area for a pore network during transient flow as well as quasi-static conditions. The capillary pressure was calculated as the average of local-scale capillary pressure (within the pores) weighted by the local interfacial area. They also compared the interfacial area surfaces obtained under quasi-static and transient conditions, and obtained results similar to *Bottero* [2009]. Although there was some difference between quasi-static and transient interfacial area surfaces, they considered the differences to be negligible.

While there has been much work on the study of interfacial area surface (equation (5)), there has been very little research related to the terms appearing in equations (3) and (4). The macroscale velocity of fluid-fluid interfaces and its evolution with time (and/or saturation) have been studied only computationally, by means of dynamic pore-network models [*Lam and Horvath*, 2000; *Nordhaug et al*., 2003; *Joekar-Niasar and Hassanizadeh,* 2012]. *Joekar-Niasar and Hassanizadeh* [2011] found that the macroscale interfacial velocity has a linear relationship with the rate of change of saturation. They also calculated coefficients k^{wn} and ψ^{wn}, and plotted them as a function of saturation. But, up to now, there has been no experimental study of any of those quantities. In this work, we present the first experimental results on the determination of w^{wn}, E^{wn}, k^{wn}, and ψ^{wn}.

1.2. Micromodels and Two-Phase Flow

An overview of various issues related to micromodels and their use in two-phase flow studies, such as network generation, fabrication materials and methods, visualization methods, and different applications, was given in *Karadimitriou and Hassanizadeh* [2012]. They defined a micromodel as "an artificial representation of a porous medium, made of a transparent material. This fluidic device bears a pore network, with features on the microscale, and an overall size of up to a few centimeters."

Micromodels have been mostly used in studying displacements of two immiscible fluid phases in porous media [*Avraam et al*., 1994; *Baouab et al*., 2007; *Chang et al*., 2009; *Corapcioglu et al*., 2009; *NagaSiva et al*., 2011; *Blois et al*., 2013; *Zhang et al*., 2013a, 2013b]. Processes of drainage and imbibition, as well as the mechanisms that dominate them, like viscous or capillary fingering and snap-off, have been studied using micromodels [*Zhang et al*., 2011; *Ferer et al*., 2004; *Grate et al*., 2010; *Gutiérrez et al*., 2008; *Hug et al*., 2003; *Rangel-German and Kovscek*, 2006; *Huh et al*., 2007]. Recently, two-phase flow studies were performed using photo-resist micromodels that had flow patterns based on stratified percolation [*Cheng*, 2002; *Pyrak-Nolte et al*., 2008; *Cheng et al*., 2004; *Chen et al*., 2007; *Liu et al*., 2011]. In those studies, distributions of the two phases in the pore network during quasi-static drainage and imbibition were visualized. Phase saturation and interfacial area could be determined using image processing, and the relationship between phase saturation, capillary pressure, and specific interfacial area under quasi-static conditions was investigated.

1.3. Present Study

The main objectives of this study were to visualize and investigate pore-scale movement of phases and interfaces under transient conditions and to determine new macroscale (average) interfacial quantities under transient conditions. We performed our experiments in an elongated micromodel, using a custom-made visualization setup. One difficulty with micromodel studies is that the macroscale capillary pressure

cannot be measured experimentally. One can measure macroscale fluid pressures by using selective pressure transducers [e.g., as in *Bottero et al*., 2011]. But, under transient conditions, the difference in macroscale fluid pressures is not equal to macroscale capillary pressure. So, an important question is how to determine macroscale capillary pressure in transient experiments. Under static conditions, the pore pressure of each phase can be assumed to be constant everywhere and equal to the pressure of its corresponding boundary reservoir. This means that the local capillary pressures at fluid-fluid interfaces—and thus the average capillary pressure—are all equal to the difference in boundary reservoirs pressures. But, this cannot be assumed under transient flow conditions. Pressures of fluids within the pores vary with time and space. Capillary pressures at different interfaces will be different from each other and will not be equal to the difference in boundary reservoirs pressures. Currently, there is no easy way of measuring local pressure or capillary pressure within the pores. But, we can determine the local capillary pressure at an interface from its curvature using Young-Laplace equation. This requires knowing the two principal curvature radii of the interface. But, our visualization method provides planar images only. So, only the planar curvature can be determined from image processing because there is no optical way of visualizing the micromodel in depth. Commonly, researchers have assumed the in-depth radius of curvature to be equal to half the depth of the micromodel [*Cheng et al*., 2004; *Chen et al*., 2007; *Pyrak-Nolte et al*., 2008]. This means that the contribution to the local capillary pressure was assumed to be the same for all interfaces (as the micromodel depth is constant everywhere). But, this is an approximation that can introduce many inaccuracies, especially for wider pores where the depth would be the dominant dimension. In this work, we determine the hidden curvature differently, with the only assumption being that the contact angle is the same in both directions, as explained shortly. We have done this by using images of the fluids distribution at any given time. After determining local-scale capillary pressures for all interfaces at a given time, we followed the approach of *Joekar-Niasar and Hassanizadeh* [2012] and obtained the macroscale capillary pressure as the area-weighted average of local-scale capillary pressures. At the same time, using pore-scale images, we determine (average) specific interfacial area and saturation over the same REV. These results are used to obtain interfacial area surfaces (P^c-S^w-a^{wn} surfaces) under different transient conditions. These are then compared to each other and to the quasi-static P^c-S^w-a^{wn} surfaces, which had been obtained for the same micromodel.

Because the movement of interfaces in time and space was monitored, we could also determine the macroscale velocity of fluid-fluid interfaces. By doing the averaging over moving REV domains along the whole micromodel, we could determine the macroscale interfacial velocity as a function of time and space. These results were used to determine material coefficients k^{wn} and ψ^{wn} as a function of saturation. Furthermore, the rate of production of interfaces within an REV was calculated under transient conditions. These results show the dependence of macroscale interfacial velocity and production rate of interfaces on saturation and its rate of change. This is the first time that such macroscale two-phase flow properties have been determined experimentally.

2. Experimental Setup

The experimental setup consisted of the micromodel, a visualization system to track the movement of the interfaces over the whole network at any given time, and a pressure measurement system that measures the external pressures at the boundaries. A brief description of various parts is given below. For more details, please refer to *Karadimitriou et al*. [2012].

2.1. Micromodel

The micromodel used in this work was the same micromodel used in the work of *Karadimitriou et al*. [2012]. It was an elongated PDMS micromodel, with overall dimensions of the pore network being 5×30 mm^2. The pore network topology was generated using Delaunay triangulation, as it is considered to be a good approximation to a natural porous medium [*Heiba et al*., 1992]. Pore bodies were cylinders and the pore throats were parallelepipeds. In planar view, pore bodies were seen as circular and pore throats as rectangular. All pore elements had a rectangular cross section. The pore network had a total of 3000 pore bodies and nearly 9000 pore throats. The pore network depth was constant everywhere and it was measured to be 40 μm. We have determined the size of an REV to be around 5×7 mm^2 [*Karadimitriou et al*., 2013]. So, our pore network was considered to be nearly 4 times the size of an REV. The micromodel was silanized before its use so as to make it uniformly and stably hydrophobic.

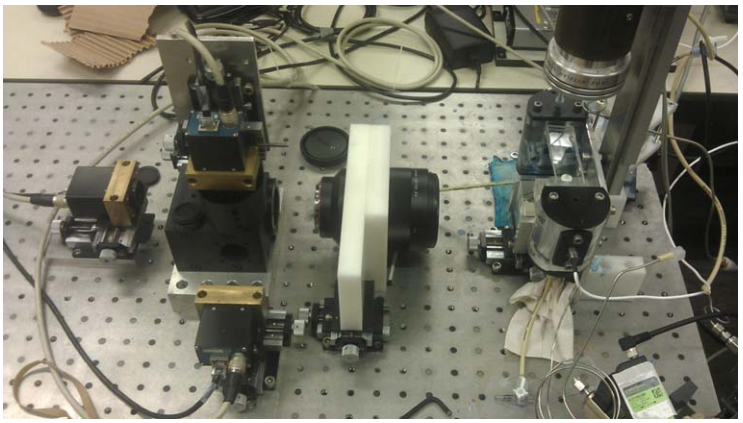

Figure 1. The experimental setup for the visualization of the elongated micromodel: (1) LED light source mounted with an objective lens. (2) Prism. (3) Magnifying lens. (4) Box with three beam splitters. (5) High-resolution CMOS cameras. The micromodel is labeled A and the inflow/outflow reservoirs are designated by B and C, respectively.

2.2. Visualization System

The whole experimental setup is shown in Figure 1. It consists of the visualization system and pressure measurement components. The visualization system is actually an open-air microscope. Major components of the optical setup were (number refers to parts shown in Figure 1): (1) a collimated LED light source mounted with an objective lens F 3.2/105 mm, (2) a prism (Edmund Optics) with dimensions of 50 mm $\times$ 50 mm, (3) a SONY Sonnar F1.8/135 mm magnifying lens, (4) a box containing three beam splitters (Edmund Optics) with dimensions of 35 mm $\times$ 35 mm, and (5) four 5-Megapixel cameras (Prosilica GC-2450). The micromodel designated with (A) was placed horizontally on a stage between the light source and the prism. The input and output holes of the micromodel were aligned with the holes of an inflow reservoir designated with (B) and an outflow reservoir designated with (C), respectively. The beam splitters created four identical images of the pore network and its fluids. The images were captured by four cameras, each focusing on one fourth of the pore network. Thus, the whole network and fluids distribution could be monitored continuously.

2.3. Pressure Measurement and Control

As immiscible fluid phases we used water and Fluorinert (FC-43). Fluorinert is a colorless, fluorine based, and inert liquid (refraction index, n = 1.291). It is 4.7 times more viscous, and 1.86 times heavier, than water ($\mu = 4.7 \times 10^{-3}$ Pa*s, $\rho = 1860$ Kg/m^3). The interfacial tension between water and Fluorinert is 58 mN/m. Because PDMS is a hydrophobic material, water was the nonwetting phase and Fluorinert was the wetting phase. Reservoirs B and C (see Figure 1) were filled with Fluorinert and water, respectively. At exactly the same level as the level of the micromodel, two pressure transducers (Kulite XTL-190M-0,7B-D) were installed, one in each reservoir, to measure the fluid pressures. These transducers were connected to a differential pressure controller (Bronkhorst), and the pressure controller was connected to a computer. In this way, it was possible to set, measure, and control the differential pressure between the two reservoirs at any instant. The controller was calibrated in a way that the maximum pressure difference that could be measured was 27 kPa, with an accuracy of 25 Pa. The pressure controller was used to adjust the pressure in the nonwetting phase reservoir. The pressure in the wetting phase reservoir was always atmospheric. By increasing the pressure of the nonwetting phase reservoir, drainage could be initiated. At the end of, or during, a drainage event, imbibition could be brought about by reducing the pressure of the nonwetting phase reservoir.

2.4. Limitations of the Micromodel

In a granular porous medium, there is a three-dimensional network of corners, through which the wetting phase remains connected and can flow out to the wetting phase reservoir. This can lead to a low irreducible wetting phase saturation. This is not the case with the quasi-two-dimensional micromodels, such as the one used in our experiments. The solid phase that is separating pores forms islands (see solid triangles in Figure 2). The corners formed around the edges of an island and top/bottom sides of the micromodel are not

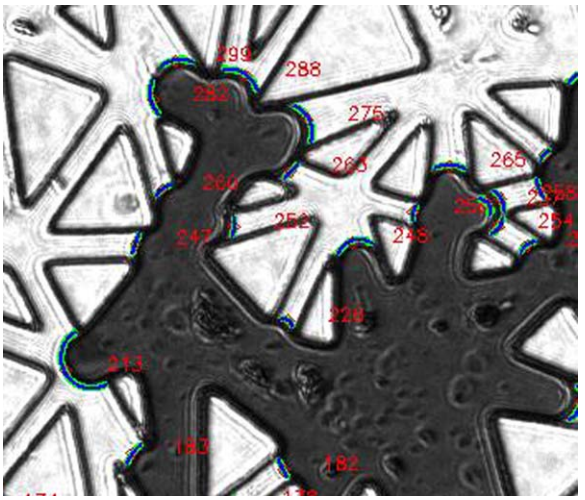

Figure 2. Image from a part of the pore network where phases and interfaces are clearly identifiable. Triangular elements are solid phase; light-colored pores are filled with the wetting phase (Fluorinert); dark-colored pores are filled with water dyed with ink; interfaces are designated with a number.

connected to the corners of other islands. So, the corner flow of wetting phase is not possible. The only parts of the network where the wetting phase stays connected with the wetting phase reservoir are the corners along the side boundaries of the network. But, the flow through these side boundary corners is quite limited, because of their limited volume. Due to the absence of corner flow, quasi-two-dimensional micromodels exhibit a highly hysteretic behavior. This limitation results in the wetting phase getting disconnected, and having a high irreducible saturation.

Another issue with PDMS is that it may swell when in contact with nonpolar organic liquids, and it may deform under the pressure of liquids. The swelling effect limits the choice of fluids that can be used in experiments. In our case, water and Fluorinert do not cause any swelling of PDMS. The deformation of PDMS under pressure can affect the laminar flow profile and pressure distribution within the channels. This effect was examined by *Gervais et al*. [2006] in shallow microfluidic channels. They came up with a dimensionless number for assessing the significance of this deformation, depending on the pressure drop along a channel, its width and height, and the Young modulus of PDMS. Based on this dimensionless number, we determined that the deformation of PDMS in our experiments can be neglected for the range of pressures that we applied.

3. Transient Experiments

3.1. Experimental Procedure

The micromodel was initially saturated with the wetting phase, namely Fluorinert (FC-43), at atmospheric pressure. Because we worked with gauge pressure, this was considered to be zero pressure. The pressure of the nonwetting phase (i.e., water) reservoir was increased to a specific value, large enough in order to cause the primary drainage of Fluorinert. The nonwetting phase started to enter the pore network, displacing the wetting phase. The spatial configuration of the fluids in the micromodel was continuously monitored. The drainage step was ended when the nonwetting phase broke through the wetting phase reservoir, and no change in the saturation was observable. Then, the pressure of the nonwetting phase reservoir was reduced to zero, causing main imbibition to occur. After primary drainage and main imbibition, a number of scanning experiments were performed. We performed two sets of experiments with two imposed nonwetting phase reservoir pressures: 6300 and 9500 Pa. During a transient displacement experiment with constant reservoir pressures, the flow velocity and thus capillary number changed continuously. These pressures resulted in the following maximum capillary number values: 2×10^{-5} and 6×10^{-5}, respectively. We have to point out that the initial intention was to go to even higher capillary numbers. But, this required higher pressures which would deform the micromodel. Also, the displacement process would become too fast for the visualization setup to capture sufficient number of images for the processing results to be trustworthy. All experiments were conducted in a constant-temperature room at 21°C.

3.2. Data Processing

3.2.1. P^c-S^w-a^{wn} Surface

The acquired images were analyzed with IDL software package (IT&T Visual Information Solutions) to calculate local capillary pressure, saturation, and the specific interfacial area between Fluorinert and dyed water. In planar view, the two fluid phases were easily identified (see Figure 2). Thus, with image analysis, the average fluid saturation for an REV could be determined.

Interfaces were identified as two-dimensional arcs. For each fluid-fluid interface, the position of the apex and the two points where it touched the walls of the pore network were identified. Then, a circle was fitted to these three points. The radius of the fitted circle was considered to give the radius of planar curvature of the interface. The width of the flow channel was calculated as the chord of the fitted circle. The length of an interface was calculated in two ways; either as the length of the arc within the pore, or as the length of a sequence of line segments, formed by pixels, identified directly in the image. These two lengths were compared so as to have an extra way of testing the accuracy of fitting. In Figure 2, an example of identified interfaces is shown.

Also, the contact angle between the meniscus and the wall was determined from the images. Under static conditions, all menisci that were in direct contact with the wetting phase reservoir had almost the same contact angle; nearly 4°. But, under transient conditions, the contact angles varied in time and space and depended on whether drainage or imbibition was occurring. Under drainage, the values of contact angle varied from 4° to 40°, while for imbibition, they varied from 65° to 100°.

In order to test the efficiency of our phase segmentation routine, we performed independent static experiments in a single capillary. We measured fluid pressures with transducers and calculated capillary pressure. We also calculated the value of capillary pressure based on image processing. The average difference between values of capillary pressure obtained with the two methods was less than 3%.

As explained above, the planar curvature radius, denoted by r_1, was determined from images for each and every interface. This was then used to calculate the contact angle from the following relation:

$$\cos\theta = \frac{w}{2r_1} \tag{6}$$

where w is the pore width. We assumed that the contact angle θ was the same in both directions. Therefore, the in-depth radius of curvature was obtained from the following equation:

$$r_2 = \frac{d}{2\cos\theta} \tag{7}$$

where d is the pore depth. Substitution of these radii of curvature in the Young-Laplace equation resulted in the following expression for local capillary pressure:

$$p^c = \sigma \cdot \left(\frac{1}{w} + \frac{1}{d}\right) \cdot \frac{w}{r_1} \tag{8}$$

The area of a single interface was calculated from the following equation, whose derivation is given in Appendix A:

$$A = \frac{w \cdot d}{\cos^2\theta} \cdot \left(\frac{\pi}{2} - \theta\right)^2 \tag{9}$$

Then, the average fluid-fluid specific interfacial area for an REV was calculated as follows:

$$a^{wn} = \frac{A^{wn}}{V_{REV}} = \frac{\sum_{i=1}^{N} A_i}{W \cdot L \cdot d} \tag{10}$$

where $W = 5$ mm and $L = 7$ mm are the overall width of the pore network and length of an REV, respectively; N is the total number of interfaces within the REV at a given time.

Then, the average capillary pressure of the collection of all interfaces within an REV was calculated as follows:

$$P^c = \frac{\sum_{i=1}^{N} p_i^c \cdot A_i}{\sum_{i=1}^{N} A_i} \tag{11}$$

Average saturation, average specific interfacial area, and average capillary pressure were determined for moving averaging windows (REVs) with dimensions 5 mm by 7 mm at any given time, and for each drainage, imbibition, and scanning experiment. At any given time during an event, the averaging window was

moved along the pore network by 300 pixels, equal to 840 μm. This led to a large number of P^c-S^w-a^{wn} data points, which allowed us to construct interfacial area surface (P^c-S^w-a^{wn} surface) under transient conditions.

3.2.2. Interfacial Area Production Term and Interfacial Conductivity

The macroscale evolution of fluid-fluid interfacial area is given by equations (3) and (4). In this section, we explain how various terms in these equations are evaluated using image analysis; leading to the determination of E^{wn}, k^{wn}, and ψ^{wn}. As explained above, the specific interfacial area, a^{wn}, was determined as a function of time and position along the pore network. So, $\frac{\partial a^{wn}}{\partial t}$ could be calculated as a function of time and space.

Next, the macroscale velocity of interfaces was determined. To this end, first, the centroid of all interfaces within the averaging window at any given time was calculated. Then, the macroscale interfacial velocity was calculated as the time rate of change of the centroid:

$$w^{wn} = \frac{1}{t^{k+1} - t^k} \left[\left(\frac{\sum_{i=1}^{N} x_i A_i^{wn}}{\sum_{i=1}^{N} A_i^{wn}} \right) \Big|_{k+1} - \left(\frac{\sum_{i=1}^{N} x_i A_i^{wn}}{\sum_{i=1}^{N} A_i^{wn}} \right) \Big|_{k} \right] \tag{12}$$

where x_i is the x coordinate of the apex of the ith interface. The two terms inside the bracket are the centroid of all interfaces within the averaging window at two consecutive time steps. Given the fact that the mass density of interfaces was assumed to be constant, these are also the center of mass of all interfaces within the averaging window. For approximation, (12) to be valid, we had to take small time steps so that not many interfaces enter or leave the averaging window of interest during the time step.

With both a^{wn} and w^{wn} known for all points along the micromodel, we calculated the divergence of product of interfacial area and its velocity, $\frac{\partial (a^{wn} w^{wn})}{\partial x}$. For this term, we employed the following approximation:

$$\frac{\partial (a^{wn} w^{wn})}{\partial x} = \frac{1}{L} \left[\sum_{i=1}^{N} (A_i^{wn} w_i^{wn}) |_{db} - \sum_{i=1}^{N} (A_i^{wn} w_i^{wn}) |_{ub} \right] \tag{13}$$

where L is the length of the averaging window, and *db* and *ub* denote the downstream and upstream boundaries of the averaging window. With $\frac{\partial (a^{wn} w^{wn})}{\partial x}$ and $\frac{\partial a^{wn}}{\partial t}$ known at any given time and position, we used equation (3) to determine E^{wn} as a function of time and position.

Next, we consider coefficients k^{wn} and ψ^{wn} in equation (4). Following the approach of *Joekar-Niasar and Hassanizadeh* [2011], ψ^{wn} was determined from quasi-static experiments, where w^{wn} was zero. Then, ψ^{wn} was obtained from the ratio of $\frac{\partial a^{wn}}{\partial x}$ and $\frac{\partial S^w}{\partial x}$ at various positions. Thereafter, with all terms in equation (4) known, except k^{wn}, we calculated it at various times and locations.

4. Results

4.1. P^c-S-A^{wn} Surface

The results obtained by image processing were used to plot average capillary pressure-saturation curves as well as average capillary pressure-saturation-specific interfacial area surfaces for the two sets of transient experiments. These data were compared to results from static experiments, for the same pore network.

In Figure 3, data points for average capillary pressure and saturation obtained for the two series of dynamic experiments as well as static experiments are shown.

The experimental data obtained under quasi-static conditions are shown in Figure 3a. The green dots in Figure 3b correspond to the set of transient experiments with maximum capillary number of 2×10^{-5}, and the red dots in Figure 3c are from transient experiments with a maximum capillary number of 6×10^{-5}. In Figure 3d, the three data sets are shown together. As it can be seen, with increase of capillary number, a larger range of saturation could be reached.

Considering the maximum and minimum values of capillary pressure obtained under different conditions, we observe that the hysteresis in capillary pressure-saturation data points is less pronounced at higher capillary numbers. This is in agreement with the findings of *Joekar-Niasar and Hassanizadeh* [2012], where a dynamic pore network model was used.

As explained in the section 1, one of our aims was to determine whether interfacial area surfaces obtained under quasi-static conditions coincide with transient interfacial area surface. In Figure 4, we plot the data

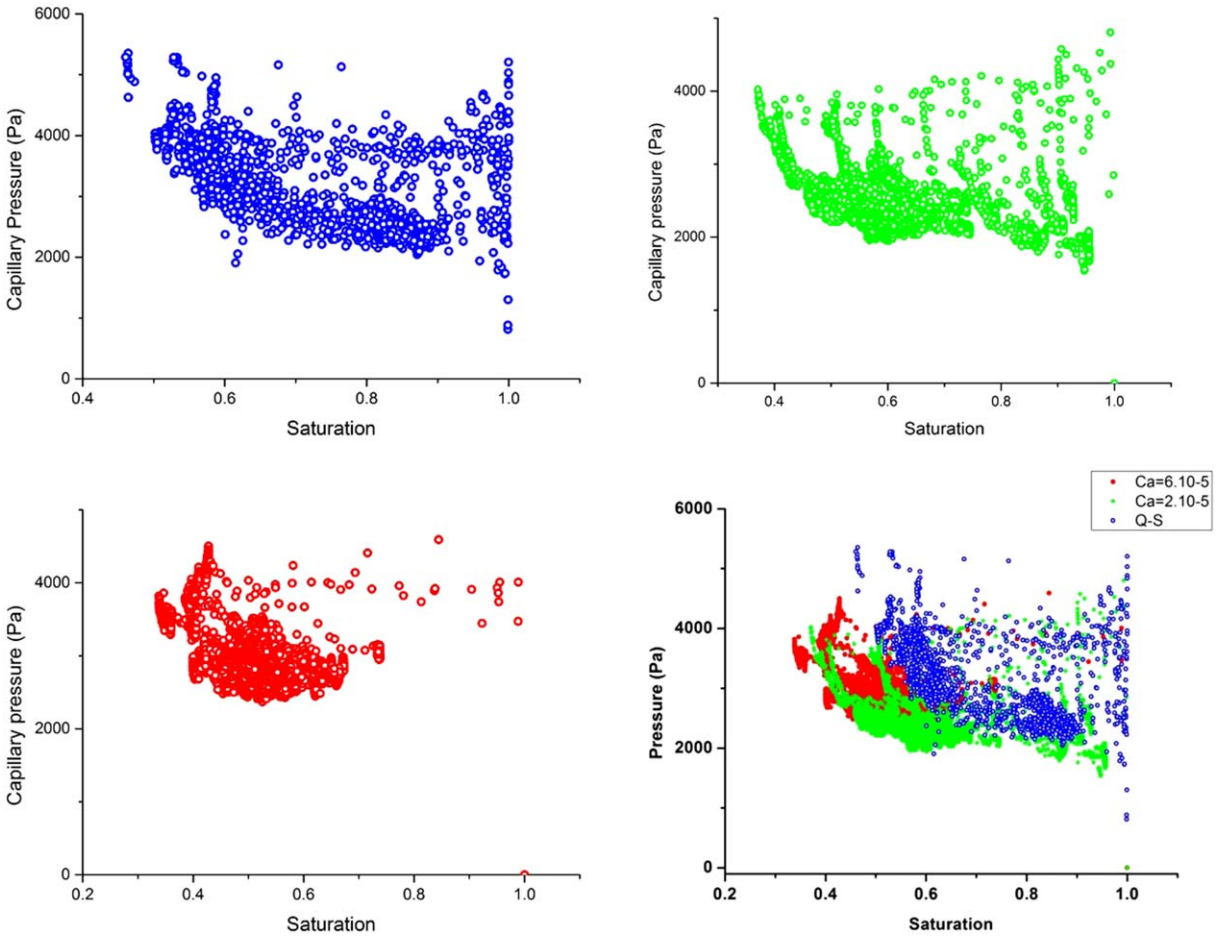

Figure 3. P^c-S^w data points for the (a) quasi-static case, (b) low capillary number, (c) high capillary number, and (d) all-in-one.

points of saturation, average internal capillary pressure, and specific interfacial area (denoted as SIA in Figure 4) from transient imbibition and drainage experiments with a maximum capillary number of 2×10^{-5} (note that the boundary pressure is fixed, which results in a variable flow rate). The resulting interfacial area surface looks rough because the data points are simply linearly connected. A similar surface was obtained for the set of experiments with a maximum capillary number of 6×10^{-5}, as well as for quasi-static experiments. We performed a comparison of the three surfaces in the following manner.

To quantify the difference between transient and static surfaces, an interpolated interfacial area contour map was prepared for all pairs of quasi-static capillary pressure-saturation data points, and was compared to the two transient data sets. The results are shown in Figures 5a and 5b for $Ca = 2 \times 10^{-5}$ and 6×10^{-5}, respectively. The interpolated contour map for specific interfacial area of static experiments is shown in the background of the figures, where darker colors correspond to larger values of specific interfacial area. The dots correspond to the ratio of the interfacial area measured under transient conditions, at a given P^c and S^w, to the value of interfacial area obtained from the static map of the same P^c-S^w values. This ratio gives a measure of how different static and transient surfaces are. The closer its value to unity, the smaller the difference between static and transient interfacial area surfaces is. The plotted points bear a color code; green corresponds to a low ratio and red to a high ratio. As it can be seen in Figure 5, the range of data points for transient experiments is not similar. The reason is that, we could not collect many data points for high saturations during high capillary number experiments, because the process was too fast to control; so, the data points for high capillary number cases are accumulated in a narrower range of saturation (0.5–0.7).

In Figure 6, the histogram of the distribution of ratios with respect to each dynamic process is shown. The mean values for both distributions were calculated to be equal to unity. The variances of the distributions

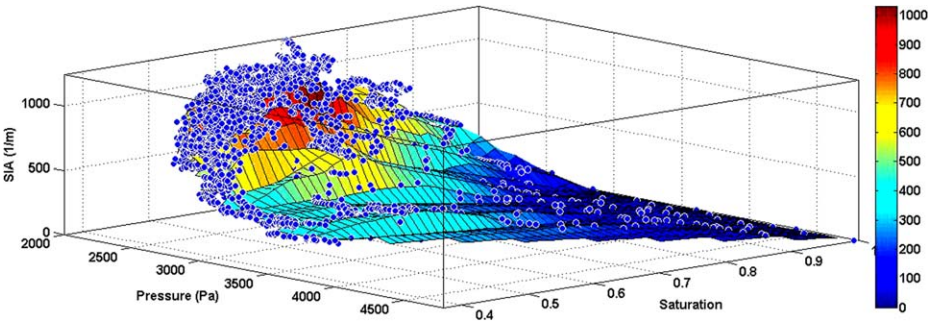

Figure 4. P^c-S^w-a^{wn} data points and the interpolated surface obtained during drainage and imbibition experiments, with nonwetting boundary gauge pressures equal to 6300 Pa and 0 Pa, respectively (corresponding to a maximum capillary number of 2×10^{-5}). The color code in the bar corresponds to the values for specific interfacial area.

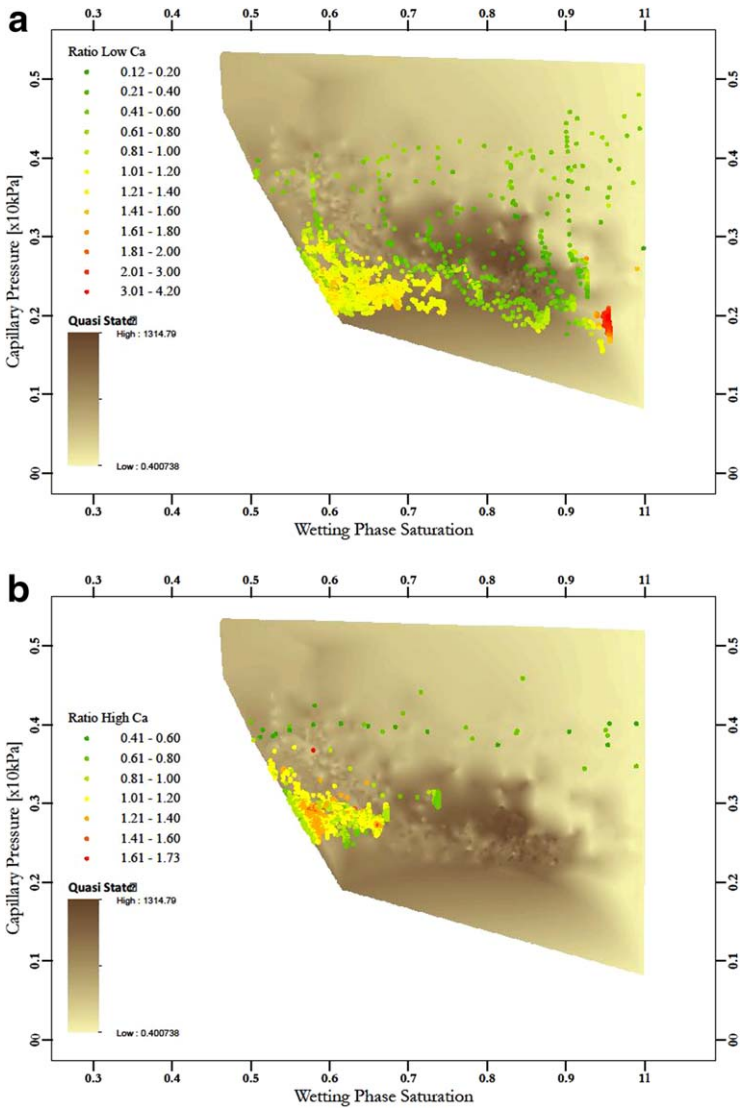

Figure 5. Interfacial area obtained from transient experiments compared to quasi-static experiments, for (a) low and (b) high capillary number experiments. The data points have a color code corresponding to the ratio of specific interfacial area obtained from transient surface to the value obtained from quasi-static surface. The contour map on the background shows interpolated values of specific interfacial based on quasi-static experiments.

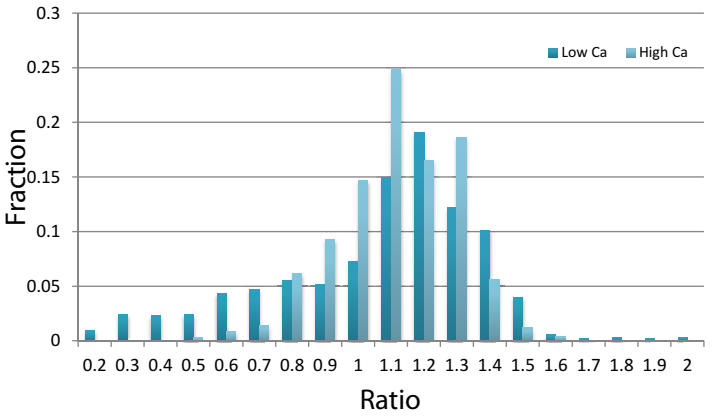

Figure 6. The histogram of the distribution of ratio of interfacial areas from transient experiments to static experiments for two different capillary numbers. The horizontal axis shows the ratio. The vertical axis gives the relative frequency.

are 0.19, for the low capillary number case, and 0.03, for the high capillary number case. The main difference in the variances is the limited range of data points obtained for the high capillary number case, as mentioned earlier. This makes it obvious that the three surfaces do not collapse to a single, unique surface.

From the interpretation of Figures 5 and 6, along with thorough examination of individual images, we made the following observations, which explain the difference between the surfaces. Under primary drainage conditions, the specific interfacial area values in both transient cases are smaller than the quasi-static value at the same capillary pressure and saturation. But, with decrease of saturation, and within the main loop of capillary pressure-saturation curves, the specific interfacial area under transient conditions is equal to, or higher, than under quasi-static conditions. Under imbibition conditions, the nonwetting phase would get disconnected. For the same saturation, with increasing capillary number, the nonwetting phase would form an increasingly larger number of disconnected blobs. For a larger number of blobs, specific interfacial area will be larger, deviating significantly from the quasi-static case.

One would expect the average capillary pressure under primary drainage to be at least equal to, if not higher than, the average entry capillary pressure of the pores and throats of the pore network. Instead, the average capillary pressure measured for primary drainage under transient conditions was lower than the one under quasi-static conditions. The reason is that under quasi-static conditions, all interfaces are at rest with the maximum possible curvature dictated by the boundary pressures. However, under transient conditions, all the interfaces do not have the same curvature at a given time. As soon as the curvature of an interface is large enough to fill new pores, the interfaces behind it get relaxed and this causes decrease of curvature at the interfaces. Thus, in average, a pressure lower than the entry capillary pressure is possible during primary drainage.

By identifying the moving interfaces for which the wetting phase was directly connected to its reservoir, we found that the average capillary pressure of these interfaces was close to the externally applied one (figure not shown here). But the average capillary pressure obtained for all other interfaces was lower.

During main imbibition, the interfaces that are located at the invading front can relax and their capillary pressure drops, while the interfaces which are located away from the front do not yet react to this change,

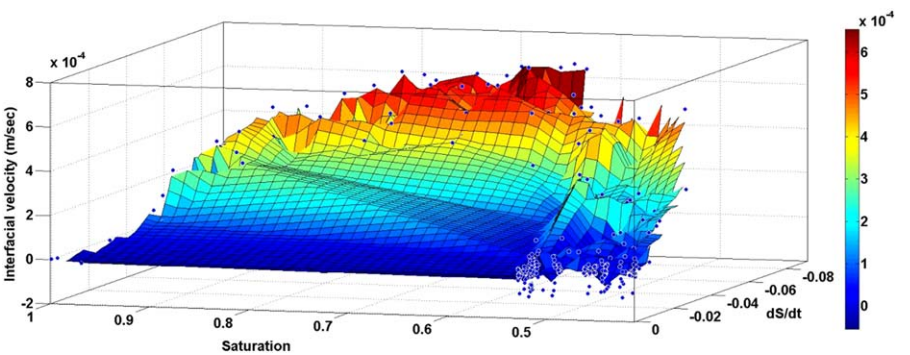

Figure 7. Interfacial velocity plotted versus saturation and its rate of change.

Table 1. The Fitting Parameters for the Macroscale Interfacial Velocity, Along With R^2, Are Given for the Experiment With a Maximum Capillary Number of 2×10^{-5}

Parameter	Value (m)
a	2.44×10^{-2}
b	3.86×10^{-2}
c	8.9×10^{-3}
$R^2 = 0.99$	

since the high viscous forces will not allow for spontaneous relaxation, and these maintain their capillary pressure. Eventually, parts of the nonwetting phase become disconnected, and form interfaces which are under high capillary pressure. This leads to an average capillary pressure under main imbibition which is higher than the one under static conditions.

During drainage scanning steps after main imbibition, the disconnected nonwetting phase reconnects quite fast. As soon as the nonwetting phase reconnects, the wetting phase saturation decreases, but the average capillary pressure does not increase drastically. Because of reconnection, the nonwetting phase propagates into the pore network as it grows in volume. So, the nonwetting phase is present and connected in the pores and throats without having to overcome the entry pressures. In a short time, it reaches the wetting phase reservoir, and then there is no reason for further increase of the average capillary pressure, since there is a connected path from the nonwetting reservoir to the outlet of the micromodel.

4.2. Production Term and Interfacial Velocity

As explained earlier, the application of the moving averaging window (see section 3.2) to the acquired images led to the calculation of S^w, a^{wn}, and w^{wn} as a function of time and space. This allowed us to calculate the right side of equation (3), namely the net rate of production of interfacial area, E^{wn}, as well as the material coefficients in equation (4), and plot them as a function of saturation and/or its rate of change. Results for the experiments with a maximum capillary number of 2×10^{-5} are plotted below and explained.

First, consider the macroscale interfacial velocity, w^{wn}, plotted in Figure 7 as a function of S^w and $\frac{\partial S^w}{\partial t}$. The resulting surface is rough because we have simply connected the data points to each other linearly. Fitting of the experimental data resulted in the following approximate equation:

$$w^{wn} = -(aS^{w2} - bS^w - c) \cdot \frac{\partial S^w}{\partial t} \tag{14}$$

where the values for the fitting parameters a, b, c, are given in Table 1.

From Figure 7, we can see that as the saturation starts to become less than one, macroscale velocity (shown by black dots) increases, reaching its maximum value at intermediate saturations. As saturation continues decreasing, interfacial velocity decreases too, eventually reaching zero. This behavior is due to the increased possibility for the creation of invasion sites (and movement of interfaces) at intermediate saturations. When saturation is close to one, or to the residual wetting phase saturation, there are not many pores available to be invaded, thus the interfacial velocity goes to zero. As saturation starts to decrease, more pores become available to be filled with the nonwetting phase. This causes the interfacial velocity to increase. At intermediate saturation, it reaches its maximum value. As saturation continues to decrease, fewer pores become

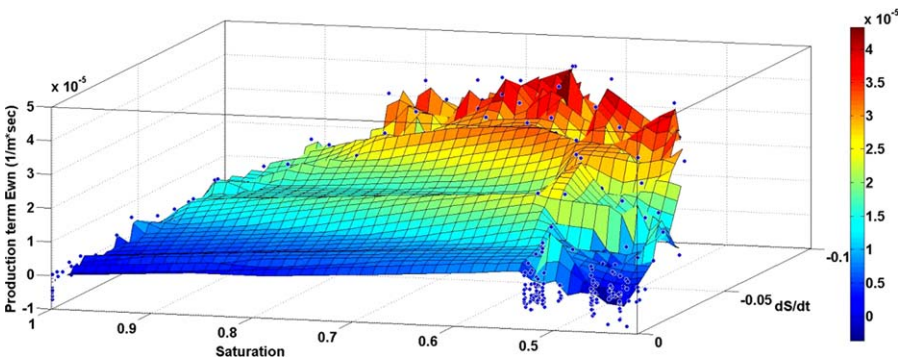

Figure 8. Interfacial production term plotted versus saturation and its rate of change.

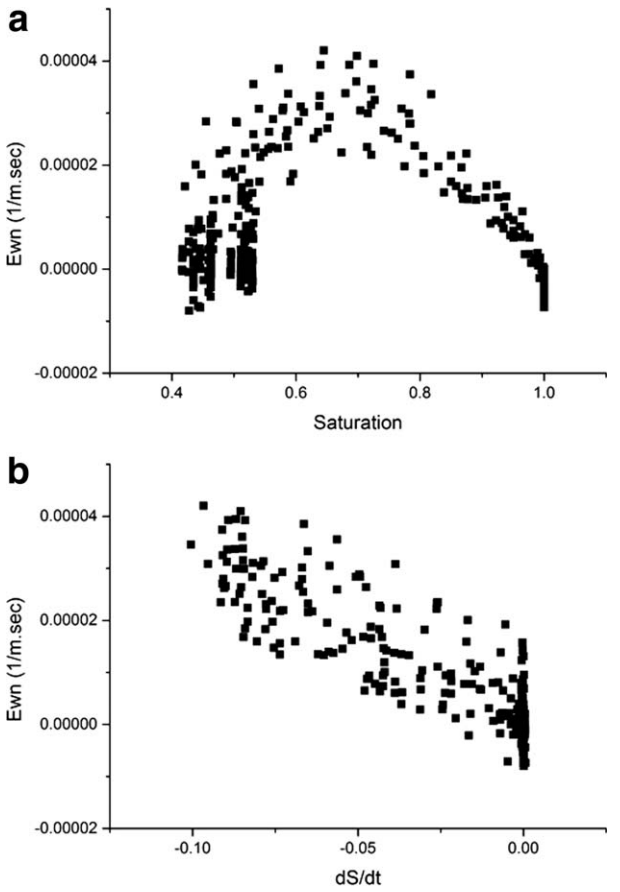

Figure 9. Production term plotted versus (a) saturation and (b) rate of change of saturation.

available to be invaded. This causes the interfacial velocity to decrease, eventually reaching zero. The same general behavior was observed for experiments at higher capillary number, with the only difference being that the interfacial velocity was larger for higher capillary numbers, as expected.

Next, the interfacial production term E^{wn}, is plotted as a surface against S^w and $\frac{\partial S^w}{\partial t}$ in Figure 8, and then separately versus S^w and versus $\frac{\partial S^w}{\partial t}$, as shown in Figure 9.

The data could be nicely fitted with the following formula:

$$E^{wn} = -\left(eS^w - fS^{w2} - g\right) \cdot \frac{\partial S^w}{\partial t} \qquad (15)$$

where the fitting coefficients e, f, g are given in Table 2. One has to keep in mind that the empirically fitted equations (14) and (15) are only valid for the given range of saturations (from 0.35 to 1) and for the specific pore network.

The experimental results obtained for interfacial velocity and interfacial production term are qualitatively in accordance with the findings of *Joekar-Niasar and Hassanizadeh* [2011]. In their work, they also found that the production term and interfacial velocity have a linear dependency on the rate of change of saturation, and they show a parabolic dependency on saturation.

Finally, the material coefficients ψ^{wn} and k^{wn}, which appear in the interface equation of motion, were calculated. Results are plotted against saturation in Figure 10. The relationships between ψ^{wn} and k^{wn} are also qualitatively the same as those obtained by *Joekar-Niasar and Hassanizadeh* [2011] from pore-network modeling.

5. Conclusions

This is the first experimental work enabling us to study the role of interfacial area as a separate state variable in two-phase flow under transient flow conditions. Also, new variables such as interfacial velocity, material coefficients, and interfacial production rate are determined. By using an elongated PDMS micromodel, the hypothesis that capillary pressure-saturation-specific interfacial area data points should form a unique surface for drainage and imbibition under quasi-static and transient flow conditions has been investigated. In our analyses, the macroscale capillary pressure has been defined based on averages of the capillary pressure of individual menisci, which is calculated from the curvature of the interfaces. Observations show that with the increase of capillary number, the difference between drainage and imbibition curves (i.e., capillary hysteresis) decreases

Table 2. The Fitting Parameters for Production Term, Along With R^2, are Given for the Experiment With a Maximum Capillary Number of 2×10^{-5}

Parameter	Value (m^{-1})
e	8.7×10^{-5}
f	2.9×10^{-4}
g	5.6×10^{-4}
$R^2 = 0.99$	

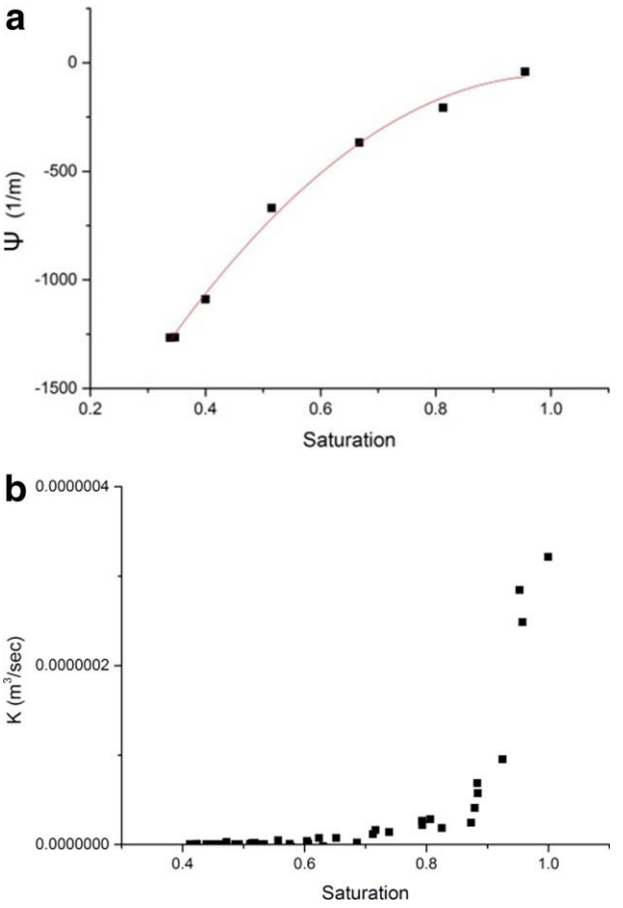

Figure 10. Material coefficients (a) ψ^{wn} and (b) k^{wn} plotted versus saturation.

significantly. Note that this effect is different from the behavior of P^n-P^w under transient conditions.

For a given capillary number, it seems that a unique P^c-S^w-a^{wn} surface can be fitted to drainage and imbibition data points. However, there is a significant difference between transient and quasi-static surfaces. This means that one interfacial area surface cannot sufficiently describe two-phase flow under transient and quasi-static conditions. There is a number of possible causes for this mismatch that require further analysis. In the original theory developed by *Hassanizadeh and Gray* [1990], it was assumed that the phases are always continuous. While, in our micromodel experiments, disconnection of the nonwetting phase is a dominant process. Furthermore, in general, the interfacial areas between the solid and the two fluid phases should be also included in the capillarity theory. Those are not considered here. Also, our results are dominated by the limitations of our two-dimensional micromodel and the topology of its pore network. Similar studies need to be performed for porous media of a more general nature.

This is the first time that the material coefficients appearing in the equation of balance of interfacial area and interfacial motion equation are determined experimentally. We have compared our results to those obtained by *Joekar-Niasar and Hassanizadeh* [2011] from pore-network modeling. Although the absolute values of parameters are different, as expected, their relationship with saturation are very much the same.

Appendix A

In Figure A1, a schematic of an interface between the wetting and the nonwetting phase in a capillary tube is presented. The capillary tube has a rectangular cross section with width w and depth d. We assume that the interface has two principal radii. Let r_1 be the radius of curvature in planar view, and r_2 in the perpendicular direction (not shown in Figure 1). We denote the contact angle between the two phases by θ.

From Figure A1, we obtain the following equation:

$$r_1 = \frac{w}{2 \cdot \cos\theta} \tag{A1}$$

$$r_2 = \frac{d}{2 \cdot \cos\theta} \tag{A2}$$

From young-Laplace equation for capillary pressure, we have:

$$p^c = \sigma \cdot \left(\frac{1}{r_1} + \frac{1}{r_2}\right) \tag{A3}$$

Substituting for r_1 and r_2, we find:

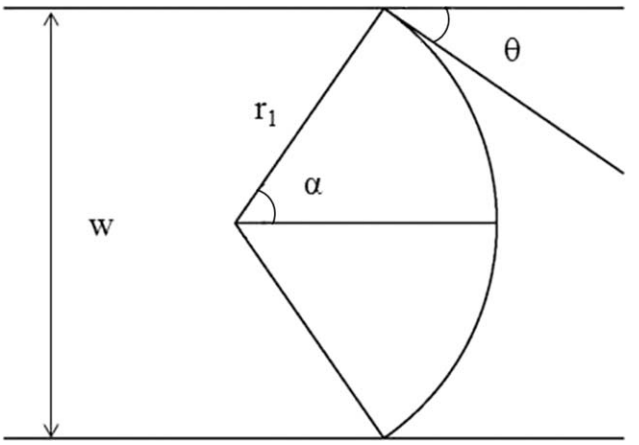

Figure A1. The sketch of an interface present in a capillary, with a rectangular cross section. Here the planar view is shown.

$$p^c = 2\sigma \cdot \left(\frac{1}{w} + \frac{1}{d}\right) \cdot \cos\theta \qquad \text{(A4)}$$

Finally, by substituting $\cos\theta$ from equation (A1), we get an expression for local capillary pressure in terms of known constants (σ and d) or variables obtained from image processing (w and θ):

$$p^c = \sigma \cdot \left(\frac{1}{w} + \frac{1}{d}\right) \cdot \frac{w}{r_1} \qquad \text{(A5)}$$

The area of an interface is given by the product of the two arc lengths. In this case, the two arc lengths are given by the following equations:

$$L_1 = r_1 \cdot 2 \cdot \left(\frac{\pi}{2} - \theta\right) \qquad \text{(A6)}$$

and

$$L_2 = r_2 \cdot 2 \cdot \left(\frac{\pi}{2} - \theta\right) \qquad \text{(A7)}$$

Then, the local interfacial area is equal to:

$$A^{wn} = L_1 \cdot L_2 = 4 \cdot r_1 \cdot r_2 \cdot \left(\frac{\pi}{2} - \theta\right)^2 \qquad \text{(A8)}$$

By substituting in equation (A8), the expressions for r_1 and r_2 from equations (A1) and (A2), respectively, we get and equation for local interfacial area where all parameters are either known, or can be calculated by image processing.

$$A^{wn} = \frac{w \cdot d}{\cos^2\theta} \cdot \left(\frac{\pi}{2} - \theta\right)^2 \qquad \text{(A9)}$$

Acknowledgments
The authors would like to acknowledge three anonymous reviewers and the Editor for valuable comments and suggestions. The first two authors are members of the International Research Training Group NUPUS, financed by the German Research Foundation (DFG) and the Netherlands Organization for Scientific Research (NWO). This research project was financed by NWO grant 818.01.008. The data from this work can be accessed upon request, by sending an email to the corresponding author.

References

Avraam, D. G., G. B. Kolonis, T. C. Roumeliotis, G. N. Constantinides, and A. C. Payatakes (1994), Steady-state two-phase flow through planar and nonplanar model porous media, *Transp. Porous Media*, *16*(1), 75–101, doi:10.1007/BF01059777.

Baouab, Z., M. Najjari, H. Ouerfelli, and S. Ben Nasrallah (2007), Experimental study of the effects of hydraulic gradient and injected-gas flow rate on fragmentation in porous media, *J. Pet. Sci. Eng.*, *59*, 250–256.

Blois, G., J. M. Barros, and K. T. Christensen (2013), PIV investigation of two-phase flow in a micro-pillar microfluidic device, paper presented at 10th International Symposium on Particle Image Velocimetry, Delft, Netherlands.

Bottero, S. (2009), Advances in theories of capillarity in porous media, PhD thesis, Utrecht Univ., Utrecht, Netherlands.

Bottero, S., S. M. Hassanizadeh, P. J. Kleingeld, and T. J. Heimovaara (2011), Nonequilibrium capillarity effects in two-phase flow through porous media at different scales, *Water Resour. Res.*, *47*, W10505, doi:10.1029/2011WR010887.

Chang, L.-C., J.-P. Tsai, H.-Y. Shan, and H.-H. Chen (2009), Experimental study on imbibition displacement mechanisms of two-phase fluid using micro model, *Environ. Earth Sci.*, *59*, 901–911, doi:10.1007/s12665-009-0085-6.

Chen, D., L. J. Pyrak-Nolte, J. Griffin, and N. J. Giordano (2007), Measurement of interfacial area per volume for drainage and imbibition, *Water Resour. Res.*, *43*, W12504, doi:10.1029/2007WR006021.

Cheng, J.-T. (2002), Fluid flow in ultra-small capillaries, PhD thesis, Purdue Univ., West Lafayette, Indiana.

Cheng, J.-T., L. J. Pyrak-Nolte, D. D. Nolte, and N. J. Giordano (2004), Linking pressure and saturation through interfacial areas in porous media, *Geophys. Res. Lett.*, *31*, L08502, doi:10.1029/2003GL019282.

Corapcioglu, M. Y., S. Yoon, and S. Chowdhury (2009), Pore-scale analysis of NAPL blob dissolution and mobilization in porous media, *Transp. Porous Media*, *79*(3), 419–442, doi:10.1007/s11242-008-9331-8.

Ferer, M., C. Ji, G. S. Bromhal, J. Cook, G. Ahmadi, and D. H. Smith (2004), Crossover from capillary fingering to viscous fingering for immiscible unstable flow: Experiment and modelling, *Phys. Rev. E*, *70*(1), 016303.

Gervais, T., J. El-Ali, A. Gunther, and K. F. Jensen (2006), Flow-induced deformation of shallow microfluidic channels, *Lab Chip*, *6*, 500–507.

Grate, J. W., C. Zhang, T. W. Wietsma, M. G. Warner, N. C. Anheier Jr., B. E. Bernacki, G. Orr, and M. Oostrom (2010), A note on the visualization of wetting film structures and a nonwetting immiscible fluid in a pore network micro-model using a solvatochromic dye, *Water Resour. Res.*, *46*, W11602, doi:10.1029/2010WR009419.

Gray, W. G., and S. M. Hassanizadeh (1989), Averaging theorems and averaged equations for transport of interface properties in multiphase systems, *Int. J. Multiphase Flow*, *15*, 81–95.

Gray, W. G., and C. T. Miller (2006), Thermodynamically constrained averaging theory approach for modeling flow and transport phenomena in porous medium systems: 3. Single-fluid-phase flow, *Adv. Water Res.*, *29*(11), 1745–1765, doi:10.1016/j.advwatres.2006.03.010.
Gutiérrez, B., F. Juarez, L. Ornelas, S. Zeppieri, and A. López de Ramos (2008), Experimental study of gas–liquid two-phase flow in glass micro-models, *Int. J. Thermophys.*, *29*, 2126–2135, doi:10.1007/s10765-007-0305-9.
Hassanizadeh, S. M., and W. G. Gray (1990), Mechanics and thermodynamics of multiphase flow in porous media including interphase boundaries, *Adv. Water Resour.*, *13*, 169–186.
Hassanizadeh, S. M., and W. G. Gray (1993a), Thermodynamic basis of capillary pressure in porous media, *Water Resour. Res.*, *29*, 3389–3405.
Hassanizadeh, S. M., and W. G. Gray (1993b), Toward an improved description of the physics of two-phase flow, *Adv. Water Resour.*, *16*, 53–67.
Heiba, A. A., M. Sahimi, L. E. Scriven, and H. T. Davis (1992), Percolation theory of two-phase relative permeability, paper SPE 11015 presented at the 57th Annual Fall Meeting of the Society of Petroleum Engineers, New Orleans, La.
Held, R. J., and M. A. Celia (2001), Modeling support of functional relationships between capillary pressure, saturation, interfacial area and common lines, *Adv. Water Resour.*, *24*, 325–343.
Hug, T. S., D. Parrat, P.-A. Kunzi, U. Staufer, E. Verpoorte, and N. F. de Rooij (2003), Fabrication of nanochannels with PDMS, silicon and glass walls and spontaneous filling by capillary forces, paper presented at 7th International Conference on Miniaturized Chemical and Biochemical Analysts Systems, Calif.
Huh, D., K. L. Mills, X. Zhu, M. A. Burns, M. A. Thouless, and S. Takayama (2007), Tuneable elastomeric nanochannels for nanofluidic manipulation, *Nat. Mater.*, *6*, 424–428, doi:10.1038/nmat1907.
Joekar-Niasar, V., and S. M. Hassanizadeh (2011), Specific interfacial area: The missing state variable in two-phase flow?, *Water Resour. Res.*, *47*, W05513, doi:10.1029/2010WR009291.
Joekar-Niasar, V., and S. M. Hassanizadeh (2012), Uniqueness of specific interfacial area–capillary pressure–saturation relationship under non-equilibrium conditions in two-phase porous media flow, *Transp. Porous Media*, *94*, 465–486, doi:10.1007/s11242-012-9958-3.
Joekar-Niasar, V., S. M. Hassanizadeh, and A. Leijnse (2009a), Insights into the relationships among capillary pressure, saturation, interfacial area and relative permeability using pore-network modeling, *Transp. Porous Media*, *74*(2), 201–219.
Joekar-Niasar, V., S. M. Hassanizadeh, L. J. Pyrak-Nolte, and C. Berentsen (2009b), Simulating drainage and imbibition experiments in a high-porosity micromodel using an unstructured pore network model, *Water Resour. Res.*, *45*, W02430, doi:10.1029/2007WR006641.
Karadimitriou, N. K., and S. M. Hassanizadeh (2012), A review of micro-models and their use in two-phase flow studies, *Vadose Zone J.*, doi:10.2136/vzj2011.0072.
Karadimitriou, N. K., V. Joekar-Niasar, S. M. Hassanizadeh, P. J. Kleingeld, and L. J. Pyrak-Nolte (2012), A novel deep reactive ion etched (DRIE) glass micro-model for two-phase flow experiments, *Lab Chip*, *12*, 3413–3418, doi:10.1039/c2lc40530j.
Karadimitriou, N. K., M. Musterd, P. J. Kleingeld, M. T. Kreutzer, S. M. Hassanizadeh, and V. Joekar-Niasar (2013), On the fabrication of PDMS micromodels by rapid prototyping, and their use in two-phase flow studies, *Water Resour. Res.*, *49*, 2056–2067, doi:10.1002/wrcr.20196.
Lam, C. H., and V. K. Horvath (2000), Pipe network model for scaling of dynamic interfaces in porous media, *Phys. Rev. Lett.*, *7*(85), 1238–1241.
Liu, Y., D. D. Nolte, and L. J. Pyrak-Nolte (2011), Hysteresis and interfacial energies in smooth-walled microfluidic channels, *Water Resour. Res.*, *47*, W01504, doi:10.1029/2010WR009541.
Marle, C. M. (1982), On macroscopic equations governing multiphase flow with diffusion and chemical reactions in porous media, *Int. J. Eng. Sci.*, *20*(5), 643–662, doi:10.1016/0020-7225(82)90118-5.
NagaSiva, G., B. Bera, N. K. Karadimitriou, S. K. Mitra, and S. M. Hassanizadeh (2011), Reservoir-on-a-Chip (ROC): A new paradigm in reservoir engineering, *Lab Chip*, *11*, 3785–3792, doi:10.1039/c1lc20556k.
Niessner, J., and S. M. Hassanizadeh (2009), Modeling kinetic interphase mass transfer for two-phase flow in porous media including fluid–fluid interfacial area, *Transp. Porous Media*, *80*, 329–344, doi:10.1007/s11242-009-9358-5.
Nordhaug, H. F., M. Celia, and H. K. Dahle (2003), A pore network model for calculation of interfacial velocities, *Adv. Water Resour.*, *26*, 1061–1074.
Porter, M. L., M. G. Schaap, and D. Wildenschild (2009), Lattice-boltzmann simulations of the capillary pressure–saturation–interfacial area relationship for porous media, *Adv. Water Resour.*, *32*(11), 1632–1640, doi:10.1016/j.advwatres.2009.08.009.
Pyrak-Nolte, L. J., D. D. Nolte, D. Chen, and N. J. Giordano (2008), Relating capillary pressure to interfacial areas, *Water Resour. Res.*, *44*, W06408, doi:10.1029/2007WR006434.
Rangel-German, E. R., and A. R. Kovscek (2006), A micro-model investigation of two-phase matrix fracture transfer mechanisms, *Water Resour. Res.*, *42*, W03401, doi:10.1029/2004WR003918.
Reeves, P. C., and M. A. Celia (1996), A functional relationship between capillary pressure, saturation, and interfacial area as revealed by a pore-scale network model, *Water Resour. Res.*, *32*, 2345–2358.
Zhang, C., M. Oostrom, T. W. Wietsma, J. G. Grate, and M. G. Warner (2011), Influence of viscous and capillary forces on immiscible fluid displacement: Pore-scale experimental study in a water-wet micro-model demonstrating viscous and capillary fingering, *Energy Fuels*, *25*(8), 3493–3505, doi:10.1021/ef101732k.
Zhang, Q., S. M. Hassanizadeh, N. K. Karadimitriou, A. Raoof, B. Liu, P. J. Kleingeld, and A. Imhof (2013a), Retention and remobilization of colloids during steady-state and transient two-phase flow, *Water Resour. Res.*, *49*, 8005–8016, doi:10.1002/2013WR014345.
Zhang, Q., N. K. Karadimitriou, S. M. Hassanizadeh, P. J. Kleingeld, and A. Imhof (2013b), Study of colloids transport during two-phase flow using a novel polydimethylsiloxane micro-model, *J. Colloid Interface Sci.*, *401*, 141–147, doi:10.1016/j.jcis.2013.02.041.